energies

MDPI

Article

A Repetitive Control Scheme Aimed at Compensating the 6k + 1 Harmonics for a Three-Phase Hybrid Active Filter

Zhaoxu Luo [1], Mei Su [1], Jian Yang [1,*], Yao Sun [1], Xiaochao Hou [1] and Josep M. Guerrero [2]

[1] School of Information Science and Engineering, Central South University, Changsha 410083, China; luozhaoxu@csu.edu.cn (Z.L.); sumeicsu@csu.edu.cn (M.S.); yaosuncsu@gmail.com (Y.S.); houxc10@csu.edu.cn (X.H.)

[2] Department of Energy Technology, Aalborg University, Aalborg East DK-9220, Denmark; joz@et.aau.dk

* Correspondence: jian.yang@csu.edu.cn; Tel.: +86-189-7488-0556

Academic Editor: Ying-Yi Hong

Received: 4 August 2016; Accepted: 23 September 2016; Published: 29 September 2016

Abstract: The traditional repetitive controller has relatively worse stability and poor transient performance because it generates infinite gain at all the integer multiples of the fundamental frequency, and its control action is postponed by one fundamental period (T_0). To improve these disadvantages, many repetitive controllers with reduced delay time have been proposed, which can selectively compensate the odd harmonics or $6k \pm 1$ harmonics with delay time reduced to $T_0/2$ and $T_0/3$, respectively. To further study in this area, this paper proposes an improved repetitive scheme implemented in a stationary reference frame, which only compensates the $6k + 1$ harmonics (e.g., -5, $+7$, -11, $+13$) in three-phase systems and reduces the time delay to $T_0/6$. Thus compared with the earlier reduced delay time repetitive controllers, the robustness and transient performance is further improved, the waste of control effort is reduced, and the possibility of amplifying and even injecting any harmonic noises into the system is avoided to a great extent. Moreover, the proposed repetitive scheme is used in the control of a three-phase hybrid active power filter. The experimental results validate the effectiveness of the proposed repetitive control scheme.

Keywords: repetitive control; hybrid active power filter; power quality; harmonic compensation

1. Introduction

Recently, due to the widespread applications of distributed generations, adjustable speed drives, uncontrolled AC/DC rectifiers, and other nonlinear loads, the harmonic pollution in power systems is becoming increasingly more serious. The passive power filter (PPF) and active power filter (APF) are the two common solutions applied to mitigate these harmonics [1,2]. PPFs have the advantages of low-cost and high-efficiency. However, they also have some inherent drawbacks. Their compensation characteristics are strongly influenced by supply impedance and they are highly susceptible to series and parallel resonances with the supply and load impedance. The APFs, which are based on power electronics, can overcome the above drawbacks of PPFs [3,4]. Additionally, APFs are more flexible and efficient compared with PPFs. However, pure APFs usually require a PWM inverter with a large kilovolt ampere (KVA) rating. Thus, they do not constitute a cost-effective harmonic filtering solution for nonlinear loads above 500–1000 kW [5,6]. To address this issue, hybrid active power filters (HAPF) have been developed, which are composed of a small rated APF and a PPF in different configurations. Among the various viable hybrid active filter topologies, parallel hybrid active filters present a cost-effective solution for harmonic filtering and reactive power compensation of high power nonlinear industrial loads, due to the small rating of the active filter (2%–3%) of the load KVA rating [6]. Thus, they have attracted increasing attention [7–11].

Among various control strategies, repetitive control, as a kind of control method based on the internal model principle, can accurately track the periodic signal or reject periodic interference. Hence it is widely used in the harmonic compensation scheme for active filters [12–15]. The traditional repetitive control technique can generate infinite gains at all the integer multiples of the fundamental frequency, including the odd, even harmonics, and dc component. However, in most cases, the introduction of high gain for all frequencies is not necessary, as it could waste control effort and reduce the system robustness without improving system performance, even amplify irrelevant signals, and reinject distortions to systems [16]. Moreover, the control action of the traditional repetitive controller is postponed by one fundamental period (T_0), hence the transient performance is poorer. To improve the drawbacks above, and considering the fact that even harmonic components do not regularly appear in power systems, literature references [16,17] propose a repetitive control scheme aimed at compensating only the odd harmonics. This uses a negative feedback array instead of the usual positive feedback in the traditional repetitive controller. Meanwhile, the delay time of the control action is reduced to $T_0/2$. As a sequence, the control performance is improved and the convergence rate is enhanced. Furthermore, among the odd harmonics, the group of $6k \pm 1$ $(k = 0, \pm 1, \pm 2 \cdots)$ harmonic components in the electrical industry are dominant due to the wide use of uncontrolled rectifiers and six-pulse converters. Thus, many improved repetitive control schemes aiming at compensating $6k \pm 1$ harmonics have been developed [18–20]. For instance, in [18] a repetitive control scheme based on the feedback array of two delay lines plus a feed forward path is presented, which can only compensate $6k \pm 1$ harmonics and reduce the delay time to $T_0/3$; In [19], the authors propose a $6k \pm 1$ repetitive control scheme in there-phase synchronous reference frame (SRF). It has an advantage of $T_0/6$ delay time. However, it needs complex coordinate transformation and much more calculation in both the positive-rotating and negative-rotating SRFs.

Considering three-phase power systems, harmonics of the same frequency can be decomposed into positive sequence, negative sequence, and zero sequence. Generally speaking, a normal balanced three-phase system mainly contains $6k + 1$ harmonics (such as -5, +7, -11, +13), and rarely contains $6k - 1$ harmonics (such as +5, -7, +11, -13). For this reason, this paper proposes a repetitive control scheme aimed at compensating the $6k + 1$ harmonics implemented in a three-phase stationary reference frame with $T_0/6$ delay time in order that the transient performance is further improved. The $6k + 1$ repetitive controller is expressed with complex-vector notation, so that the dual-input/dual-output control system (in the $\alpha\beta$ reference frame) can be simplified into one single-input/single-output system. Meanwhile, the general design method of the $Lk + M$ repetitive controller is also introduced, with which a repetitive controller aimed at compensating $Lk + M$ harmonics can be easily deduced. Moreover, taking the transformerless parallel hybrid active filter as the controlled object, a harmonic compensating control system based on the proposed $6k + 1$ repetitive control scheme is presented. Finally, the experimental results validate the effectiveness of the $6k + 1$ repetitive control scheme.

2. System Structure and Mathematical Modeling of HAPF

2.1. Topological Structure Analysis

The topology of the transformerless parallel hybrid active filter is shown in Figure 1. It consists of an LC passive filter and a three-phase voltage source inverter (VSI). The purposes of installing the LC filter are: (1) to provide reactive power compensating and absorb some harmonics; (2) to sustain fundamental voltage at the point of common coupling (PCC). Additionally, the active filter (VSI) is responsible for improving the filtering characteristics of the passive filter and avoiding the undesirable resonances with the grid. To minimize its own KVA rating, VSI does not participate in reactive compensation, and the grid voltage is almost fully dropped on the capacitor in the LC filter. Thus the fundamental voltage sustained by VSI is small such that the dc bus voltage rating of VSI can be set very low, the KVA rating and power losses are then reduced greatly. Due to the presence of the VSI, it is not necessary that the LC filter is accurately tuned at a certain harmonic frequency. The design

objective of the LC filter is to offer the lowest possible impedance path for injecting harmonic currents, on the premise of ensuring reactive power compensating.

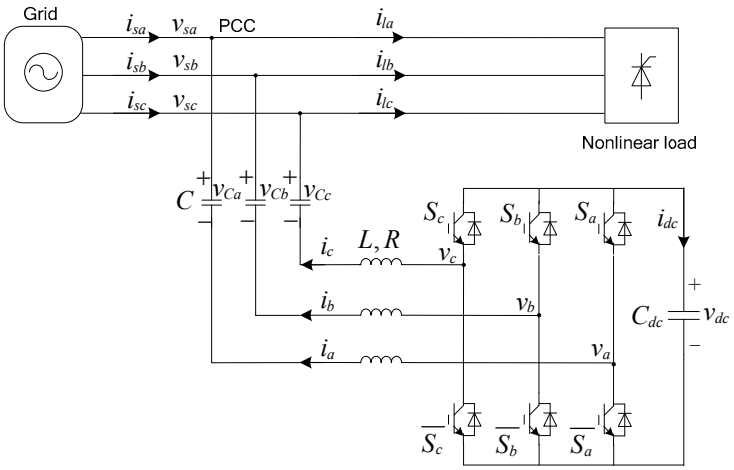

Figure 1. Topology of parallel hybrid active power filter.

2.2. Mathematical Modeling

According to Figure 1, the mathematical model in state-space representation for the system is formulated as

$$\begin{cases} L\frac{di_a}{dt} = -v_{sa} + v_{Ca} - Ri_a + v_a \\ L\frac{di_b}{dt} = -v_{sb} + v_{Cb} - Ri_b + v_b \\ L\frac{di_c}{dt} = -v_{sc} + v_{Cc} - Ri_c + v_c \end{cases} \tag{1}$$

$$\begin{cases} C\frac{dv_{Ca}}{dt} = -i_a \\ C\frac{dv_{Cb}}{dt} = -i_b \\ C\frac{dv_{Cc}}{dt} = -i_c \end{cases} \tag{2}$$

$$C_{dc}\frac{dv_{dc}}{dt} = i_{dc} = -(S_a i_a + S_b i_b + S_a i_a) \tag{3}$$

where S_a, S_b, and S_c are switching functions defined by

$$S_x = \begin{cases} 1, & (when\ \ S_x\ \text{on},\ \overline{S_x}\ \ off) \\ 0, & (when\ \ S_x\ \text{off},\ \overline{S_x}\ on) \end{cases} \qquad (x = a, b, c) \tag{4}$$

3. System Control

According to (1) and (2), it can be inferred that the state equation of the output current i_x $(x = a, b, c)$ is a second-order differential equation. If the output current control is implemented in a dq synchronous reference frame, it needs to sample and feedback the AC capacitor voltage v_{Cx} $(x = a, b, c)$ to achieve decoupling control between the d-axis and q-axis. Therefore, in this paper, the output current control is implemented in the $\alpha\beta$ stationary frame, which has the advantages of no requirements for complex decoupling control and AC capacitor voltage sampling. The overall system control diagram is shown in Figure 2, it is mainly composed of dc-link voltage control and harmonic current tacking control. In this figure, $Bpf(s)$ is a band-pass filter to extract the fundamental frequency component of the input signal, and its expression is given by

$$Bpf(s) = \frac{\gamma\omega_0 s}{s^2 + \gamma\omega_0 s + \omega_0^2} \tag{5}$$

where ω_0 is the grid frequency; γ is the control coefficient of passband width and $\gamma > 0$.

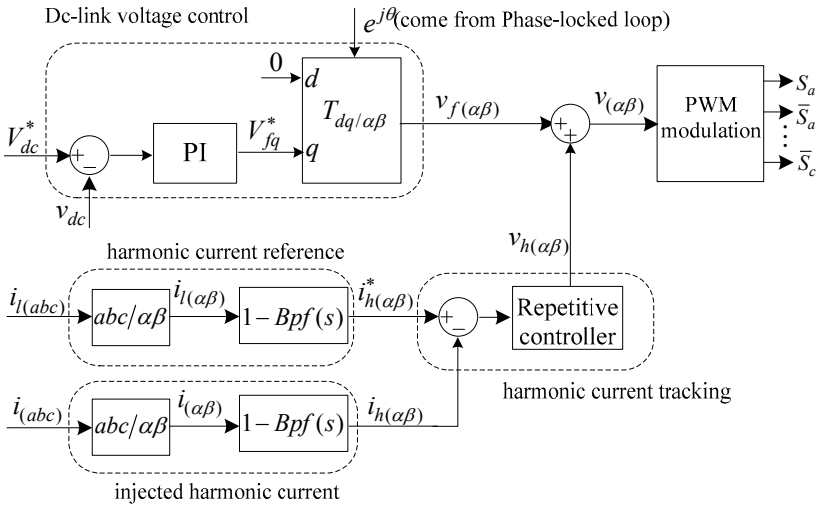

Figure 2. Overall block diagram of system control.

3.1. DC-Link Voltage Stabilization Method

Assuming that the VSI does not provide reactive power compensation for the load and only absorbs active power from the grid to maintain its power loss then according to the power conservation principle, we have

$$P_{in} = C_{dc} v_{dc} \frac{dv_{dc}}{dt} + P_{loss} \tag{6}$$

where P_{in} is the active power absorbed from the grid, $C_{dc} v_{dc} \frac{dv_{dc}}{dt}$ is the power of the dc-link capacitor, and P_{loss} is the power loss of the inverter. It can be inferred from (6) that if P_{loss} is regarded as a disturbance, v_{dc} could be controlled by adjusting P_{in}. In the dq synchronous reference frame (grid voltage orientation), the active power P_{in} and reactive power Q_{in} absorbed by VSI can be given by

$$\begin{cases} P_{in} = -\frac{V_{sd} V_{fq}}{X} \\ Q_{in} = \frac{V_{fd}^2 - V_{sd} V_{fd} + V_{fq}^2}{X} \end{cases} \tag{7}$$

where X denotes the fundamental frequency impedance of the LC filter; V_{sd} is the d-axis component of the grid voltage ($V_{sq} = 0$); V_{fq}, V_{fq} are the d-axis and q-axis components of the VSI output fundamental voltage, respectively.

It can be inferred from (7) that P_{in} is only regulated by V_{fq}. Generally, V_{fq} is small. Thus, $Q_{in} \approx 0$ could be achieved when V_{fq} is set to 0. Thus, the dc-link voltage regulator can be designed as (8), and the corresponding bode diagram is shown in Figure 2.

$$\begin{cases} V_{fq}^* = (k_p + k_i/s)(V_{dc}^* - v_{dc}) \\ V_{fd}^* = 0 \end{cases} \tag{8}$$

where V_{dc}^* is the rated value of the dc-link voltage; k_p, k_i are the parameters of the PI controller.

3.2. Harmonic Current Tracking Control

Harmonic current tracking control is the important part of system control, which contributes directly to the performance of harmonic compensating. The block diagram of current control is shown in Figure 2. Considering the case that the three-phase load current mainly contains $6k + 1$ harmonics, this paper presents a $6k + 1$ repetitive control scheme to compensate these harmonics. The detailed theoretical derivation, analysis, and design of the proposed $6k + 1$ repetitive controller is given in the next section.

4. Repetitive Control Scheme ($6k + 1$)

4.1. Internal Model of 6k + 1 Repetitive Controller

Firstly, the internal model of the well-known traditional repetitive controller is given by

$$RC_t(s) = \frac{e^{-sT_0}}{1 - e^{-sT_0}} \tag{9}$$

where e^{-sT_0} is the periodic time delay unit, and T_0 is the fundamental period, i.e., $T_0 = 2\pi/\omega_0$.

By setting the denominator $1 - e^{-sT_0}$ in (9) equal to zero, the following can be obtained

$$s_{pk} = jk\omega_0 \quad (k = 0, \pm1, \pm2, \ldots, \pm\infty) \tag{10}$$

where s_{pk} is the pole of (9). Seen from (10), it is clear that the traditional repetitive controller has an infinite number of poles located at $jk\omega_0$, which is the reason that the traditional repetitive controller has resonant peaks at every integral multiple of fundamental frequency ω_0.

In order to make a repetitive controller with poles only located at a selected group of harmonic frequencies, a new internal model needs to be structured. Assume the order h of these harmonics meets the rule:

$$h = Lk + M \tag{11}$$

where L, M are intergers, and L is not equal to zero.

Then, the poles of the new internal model should be located at

$$s'_{pk} = j(Lk + M)\omega_0 \quad (k = 0, \pm1, \pm2, \ldots, \pm\infty) \tag{12}$$

Moreover, to enhance the frequency selectivity, an infinite number of zeros of the new internal model that are located in the midpoints between two consecutive poles are introduced as

$$s'_{zk} = j(Lk + M + 0.5L)\omega_0 \quad (k = 0, \pm1, \pm2, \ldots, \pm\infty) \tag{13}$$

These zeros bring another benefit of allowing bigger gains with improved performance.

In order to satisfy (12) and (13), the general internal model for $Lk + M$ harmonics can be structured as

$$RC_g(s) = \frac{1 - e^{-\frac{(s - j\omega_0(M+0.5L))}{L}T_0}}{1 - e^{-\frac{(s - j\omega_0 M)}{L}T_0}} \tag{14}$$

After the substitution of L = 6 and M = 1 in (14), the $6k + 1$ internal model is given by

$$RC(s) = \frac{1 + e^{j\frac{\pi}{3}}e^{-s\frac{T_0}{6}}}{1 - e^{j\frac{\pi}{3}}e^{-s\frac{T_0}{6}}} \tag{15}$$

Comparing (15) with the traditional internal model given by (9), it can be found that the delay time of $6k + 1$ internal model is reduced to $T_0/6$, which means a much faster dynamic response. What is more, it should be noted that the $6k + 1$ internal model is expressed using the complex-vector notation, as it contains the complex coefficient $e^{j\frac{\pi}{3}}$. As a consequence, the input signal of RC(s) is required to be a complex vector. The block of the proposed $6k + 1$ internal model is shown in Figure 3.

Assuming that the fundamental frequency f_0 = 50 Hz, i.e., T_0 = 0.02 s, the bode plot of the $6k + 1$ repetitive controller internal model is shown in Figure 4. As expected, the amplitude-frequency response curve shows that the $6k + 1$ internal model has resonant peaks that are located at frequency multiples $6k + 1$ of 50 Hz (50, −250, 350, −550, 650 Hz...), and has notches that are located at frequency multiples $6k + 4$ of 50 Hz (−100, 200, −400, 500 Hz...). The phase-frequency response curve shows the phase shift is bound between 90° and −90°, and zero at the peaks and notches.

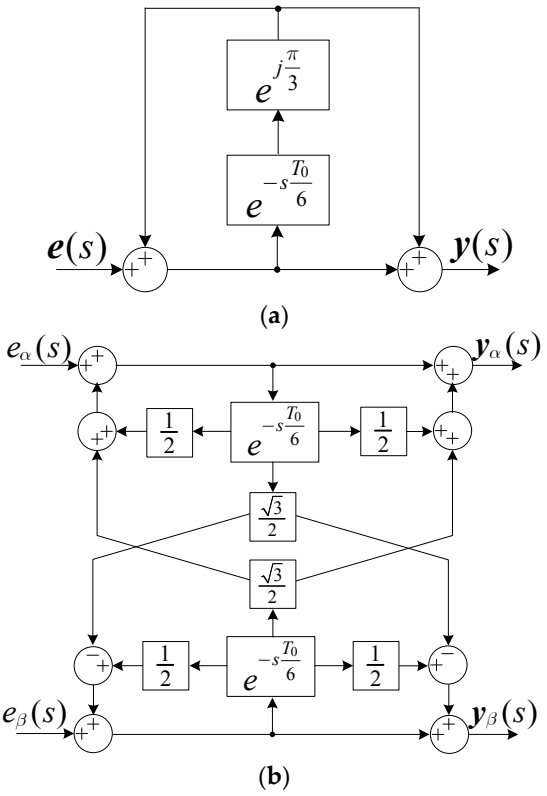

Figure 3. Block diagram of the $6k + 1$ repetitive controller internal model: (**a**) Complex-vector notation; (**b**) Scalar notation.

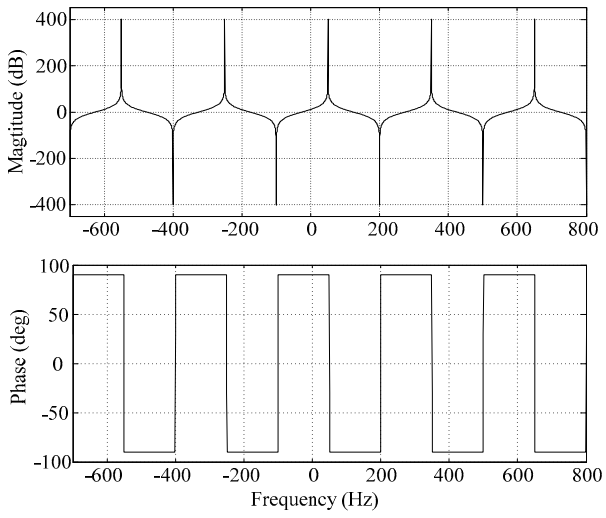

Figure 4. Bode plot of the proposed repetitive controller internal model.

4.2. Fractional Delay Compensation

In a practical application, the implementation of the repetitive control scheme is usually performed in the digital form. Using the transformation $z = e^{sT_s}$, (15) can be discretized and its expression in discrete time domain is given by

$$RC(z)\,|_{z=e^{sT_s}} = \frac{1 + e^{j\frac{\pi}{3}} z^{-\frac{N_0}{6}}}{1 - e^{j\frac{\pi}{3}} z^{-\frac{N_0}{6}}} \tag{16}$$

where T_s is the sampling period, and $N_0 = T_0/T_s$ (the number of samples per fundamental period).

In most cases, the sampling frequency f_s ($f_s = 1/T_s$) is a fixed rate (e.g., 10 kHz, 12.8 kHz, 20 kHz), and the grid frequency detected by PLL is variable in a certain range (e.g., 49–51 Hz). Thus, $N_0/6$ is usually non-integer.

Let

$$z^{-\frac{N_0}{6}} = z^{-(D+d)} = z^{-D} \cdot z^{-d} \tag{17}$$

where D and d are the integral and fractional parts of $N_0/6$, respectively.

In a common implementation, $z^{-N_0/6}$ is approximately treated as z^{-D} and performed by reserving D memory locations, with the fractional order part z^{-d} neglected. However, this will cause the resonant peaks to deviate from the harmonic frequencies. As a consequence, the harmonic compensation performance could be degraded.

To address this problem, fractional delay (FD) filters have been used as approximations of z^{-d}. The magnitude-frequency and phase-frequency characteristics of z^{-d} can be given by

$$\begin{cases} \left|z^{-d}\right| = 1 \\ \angle z^{-d} = -d\omega T_s \end{cases} \tag{18}$$

Thus, it requires that FD filters should have a unit gain and linear phase in the low-middle frequencies, and achieve a high attenuation rate in the high frequencies to enhance the system stability.

In the condition of $\left|z^{-1} - 1\right| < 1$ (i.e., $-\pi/(3T_s) < \omega < \pi/(3T_s)$), with the use of the Taylor expansion, z^{-d} can be expressed as

$$z^{-d} = (1 + z^{-1} - 1)^d = 1 + d(z^{-1} - 1) + \ldots + \frac{d(d-1)\ldots(d-n+1)}{n!}(z^{-1} - 1)^n \tag{19}$$

Specifically, choosing the first-order Taylor expansion of z^{-d} as a FD filter, that is

$$Fd(z) = 1 - d + dz^{-1} \tag{20}$$

Figure 5 shows the bode plot of $Fd(z)$, with $T_s = 78.125$ μs, d = 0.2, 0.5, and 0.8, respectively. It can be seen that $Fd(z)$ has a low-pass filter nature. At low frequencies, $Fd(z)$ has a good linear phase approximating to the ideal value. However, the main disadvantages of $Fd(z)$ are that the cutoff frequency is too high (greater than 3000 Hz), and it changes with the value of d. Only when d = 0.5, does $Fd(z)$ achieve the lowest cutoff frequency and the best linear phase.

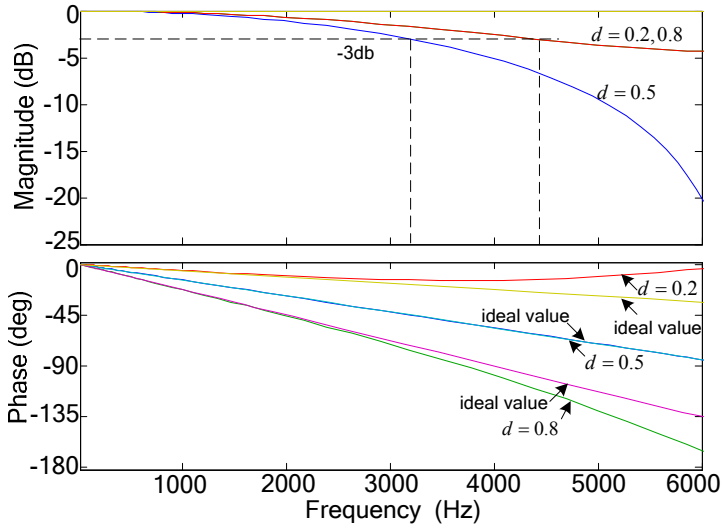

Figure 5. Bode plot of Fd(z).

To overcome the above issue, this paper presents a FD filter $Q(z)$ by cascading *Fd(z)* with a zero-phase digital low-pass filter, i.e.,

$$Q(z) = Fd(z)M(z) \tag{21}$$

where $M(z)$ is the zero-phase digital low-pass filter used to lower the cut-off frequency and increase the attenuation rate at high frequencies. Its expression is given as

$$M(z) = \left(a_1 z + a_0 + a_1 z^{-1}\right)^n \tag{22}$$

where $a_0, a_1 > 0$ and $a_0 + 2a_1 = 1$; n is the order of filter.

Although $Q(z)$ is non-causal, the time delay term z^{-D} makes it applicable. After the fractional delay compensation, (16) should be revised as

$$RC(z) = \frac{1 + e^{j\frac{\pi}{3}} Q(z) z^{-D}}{1 - e^{j\frac{\pi}{3}} Q(z) z^{-D}} \tag{23}$$

4.3. Design of 6k + 1 Repetitive Controller

Figure 6 shows the block diagram of the harmonic current tracking control. This paper adopts a plug-in repetitive controller structure in the control loop, where the PI controller is used to enhance the stability and improve dynamic response, and the repetitive controller is used to eliminate the steady-state error.

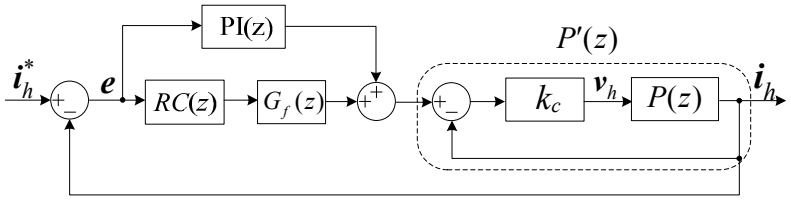

Figure 6. Block diagram of harmonic current tracking control.

In Figure 6, *P(z)* is the plant of the current control. According to (1) and (2), its expression in continuous domain can be obtained as

$$P(s) = \frac{1}{Ls + R + 1/Cs} \tag{24}$$

Obviously, *P(s)* is a second-order system. To modify the characteristic of *P(s)*, a method of output current status feedback is used. According to Figure 6, the modified plant expression is given by

$$P'(s) = \frac{k_c P(s)}{1 + k_c P(s)} = \frac{1}{\frac{L}{k_c}s + \frac{(k_c + R)}{k_c} + \frac{1}{k_c C s}} \tag{25}$$

Equation (25) reveals that $P'(s)$ can be viewed as R becomes 1 ($k_c \gg R$), while L, C become $1/k_c$ and k_c times their original values in P(s), respectively. The bode plots of $P(s)$ and $P'(s)$ are shown in Figure 7, with $L = 3$ mH, $C = 90$ μF, $R = 0.1$ Ω. As seen, $P'(s)$ has cancelled the resonant peak appearing in $P(s)$, and presents the characteristics of a band-pass filter. The passband width depends on the value of k_c. A larger k_c leads to a bigger passband width and smaller phase lead/lag.

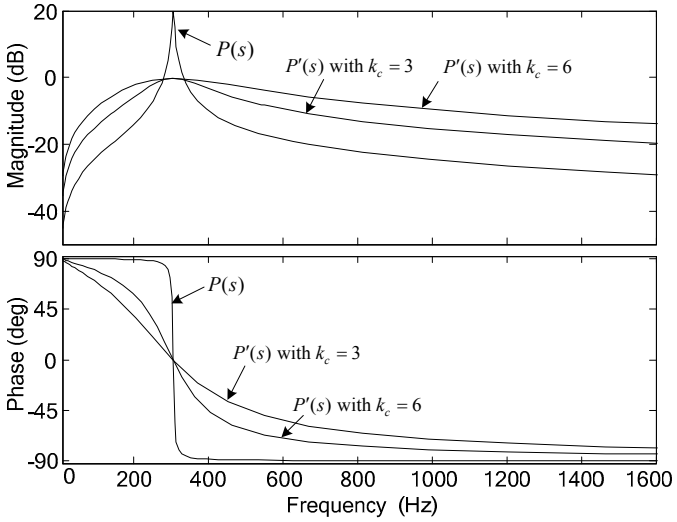

Figure 7. Bode plots of *P(s)* and $P'(s)$.

In Figure 7, without the repetitive controller, the tracking error $\boldsymbol{e}$ between the reference $\boldsymbol{i}_h^*$ and output $\boldsymbol{i}_h$ is

$$\boldsymbol{e}_0(z) = \frac{1}{1 + PI(z)P'(z)}\boldsymbol{i}_h^* \tag{26}$$

where $PI(z)$ should be designed to guarantee the stability of $\boldsymbol{e}_0(z)$.

With the proposed $6k + 1$ repetitive controller, the tracking error $\boldsymbol{e}$ can be written as

$$\begin{aligned} \boldsymbol{e}(z) &= \boldsymbol{e}_0(z)\tfrac{1}{1+H(z)G_f(z)R(z)} \\ &= \tfrac{1}{2}\boldsymbol{e}_0(z)\tfrac{(1-e^{j\frac{\pi}{3}}Q(z)z^{-D})}{1-(1-H(z)G_f(z))\,(1+e^{j\frac{\pi}{3}}Q(z)z^{-D})/2} \end{aligned} \tag{27}$$

where $G_f(z)$ is the compensation function, and

$$H(z) = \frac{P'(z)}{1 + PI(z)P'(z)} \tag{28}$$

By the small gain theorem, a sufficient condition for ensuring (27) stable can be given as

$$\left|(1 - H(z)G_f(z))\,(1 + e^{j\frac{\pi}{3}}Q(z)z^{-D})/2\right| < 1 \tag{29}$$

Clearly, $\left|(1 + e^{j\frac{\pi}{3}}Q(z)z^{-D})/2\right| \leq 1$ is true. To make (29) true, it only needs $\left|1 - H(z)G_f(z)\right| < 1$ to be satisfied. Thus, $G_f(z)$ can be chosen as

$$G_f(s) = \frac{1}{H(s)} \cdot \frac{1}{\tau s + 1} \tag{30}$$

where $G_f(s)$ and $H(s)$ are the functions of $G_f(z)$ and $H(z)$ in Laplace domain, respectively; $1/(\tau s + 1)$ is a low-pass filter.

Moreover, on the premise of system stability, it can be derived that the numerator of (27) has such a steady-state relationship:

$$1 - e^{j\frac{\pi}{3}}Q(e^{j(6k+1)\omega_0 T_s})e^{-j(6k+1)\omega_0 D T_s} = 0 \tag{31}$$

Equation (31) indicates that the $6k + 1$ repetitive control scheme can eliminate the steady-state error of $6k + 1$ harmonics tracking in D + d T_s (i.e., $T_0/6$), which means the proposed repetitive control scheme could have a much faster transient state response than the traditional one.

5. Experimental Results

To validate the correctness and effectiveness of the proposed $6k + 1$ repetitive control scheme, a prototype of a three-phase parallel hybrid APF was built in the laboratory, which is shown in Figure 8. The control system is realized by a combination of digital signal processor TMS320F28335 and field programmable gate array FPGA EP2C8T144C8N. The power switches use three Infineon IGBT modules and the drive circuit uses M57962L driver chips. The non-linear load used in the experiments is a three-phase diode rectifier bridge with resistive load. The overall experimental parameters are given in Table 1.

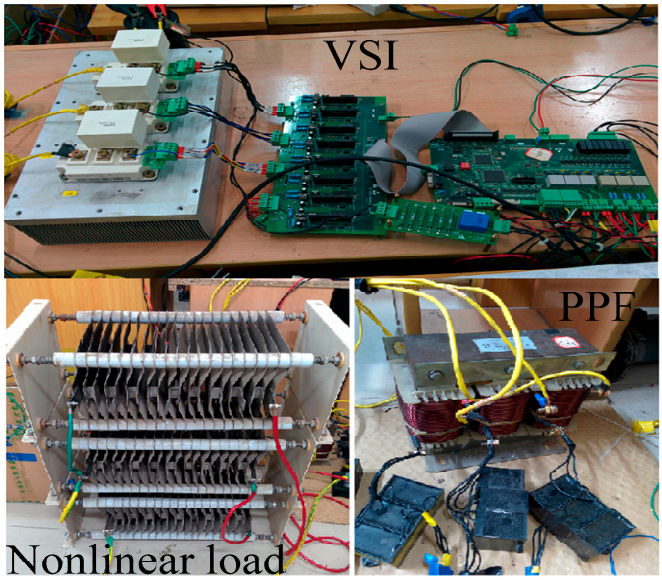

Figure 8. Photograph of the prototype.

Table 1. Experimental parameters.

Parameters	Symbol	Value	Unit
grid phase voltage	v_s	60	V (rms)
grid frequency	f	50	Hz
inductance	L	3	mH
capacitor	C	90	μF
dc bus voltage	V_{dc}	80	V
load resistance	R_L	6.6	Ω
switching period	T_s	78.125	μs

5.1. Controller Parameters

In the implementation of experiments, the parameters of the controllers are given as follows.

(1) Dc-link voltage PI controller: $k_{p1} = 2$, $k_{i1} = 5$.
(2) In the harmonic current tacking loop:

   a. The zero-phase low-pass filter $M(z)$ is given as $M(z) = (0.25z + 0.5 + 0.25z^{-1})^2$;

b. The number of delay sample is 42, and the FD filter is given as

$$Fd(z) = 1 - d + dz^{-1} = 0.333 + 0.667z^{-1} \tag{32}$$

c. Output current state feedback gain $k_c = 3$;
d. PI controller in the plug-in repetitive controller: $k_{p2} = 1$, $k_{i2} = 1$.
e. The compensation function $G_f(z)$ is given as

$$G_f(z) = \frac{5 - 9.303z^{-1} + 4.397z^{-2}}{1 - 1.677z^{-1} + 0.6766z^{-2}} \tag{33}$$

5.2. LC Filter Parameters

As the non-linear load used in this paper is a three-phase diode rectifier bridge with resistive load, the 5th, 7th, 11th, 13th harmonic currents are dominant in the load current. Assuming that the load harmonic currents are fully compensated by the hybrid APF, the voltage drop across the LC filter by the injected compensating harmonic current is

$$|v_h| = \left| \sum_{m>1} i_{lh}^m (\omega_m L - \frac{1}{\omega_m C}) \right| \leq \sum_{m>1} (I_{lh}^m \left| \omega_m L - \frac{1}{\omega_m C} \right|) \tag{34}$$

where i_{lh}^m is the m-th order harmonic component of load current, and I_{lh}^m is the amplitude of i_{lh}^m.

For the hybrid APF, the design objective of the LC filter is to offer a lowest possible impedance path for injecting harmonic currents, in other words, to minimize the voltage drop $|v_h|$. Thus, the dc-link voltage rating of VSI can be minimized.

Then, an optimization function can be given as

$$f_{\min} = \sum_{m=5,7,11,13} (I_h^m \left| \omega_m L - \frac{1}{\omega_m C} \right|) = I_f \cdot \sum_{m=5,7,11,13} (HD_m \left| \omega_m L - \frac{1}{\omega_m C} \right|) \tag{35}$$

where HD_m is the individual m-th order harmonic distortion rate, and I_{lf} is the amplitude of fundamental component in the load current.

The capacitor C in the LC filter can be chosen by the rule as follows:

$$Q_C = 3\omega_1 C V_s^2 \tag{36}$$

where Q_C is the reactive power demanded by load, ω_1 is the grid frequency, V_s is the grid voltage amplitude.

Assume the capacitor C has been determined, such as C = 90 uf. According to Figure 11b, it can be seen that $HD_5 = 22.4\%$, $HD_7 = 8\%$, $HD_{11} = 5.7\%$ and $HD_{13} = 2.6\%$. Substituting the above parameters into (32), the optimal inductor L can be determined as L = 2.8 mH. So we can choose L = 3 mH for the hybrid APF experimental prototype without loss of much performance, and the resonant frequency of the LC filter is 306 Hz.

5.3. Experimental Results

Figure 9 shows the dynamic behavior of the dc-link capacitor voltage in the start-up process. To avoid the inrush current caused by the capacitors, the series-resistance soft-start mode was used in the experiments. Specifically, when $v_{dc} \leq V_{set} = 60$ V, the IGBTs are turned off, the capacitors are charged up with small current due to the series-resistance; when $v_{dc} > V_{set}$, the series-resistance is bypassed and then the PWM pulses will be activated. v_{dc} reaches the setting value 80 V in the steady state, which verifies the correctness of the dc voltage control strategy.

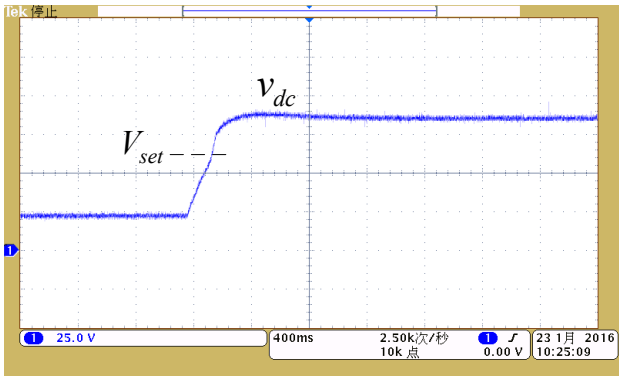

Figure 9. Start-up process of dc-link voltage.

To validate the static and dynamic performances of the proposed $6k + 1$ repetitive control scheme, the related experimental results are shown in Figures 10–13. For the sake of simplicity, only the a-phase waveforms are displayed.

Figure 10 shows the harmonic compensation results when a nonlinear load is disconnected ($i_{la} = 0$). As seen, $i_{sa} = i_a$, and i_{sa} is almost the reactive power current provided by the LC filter. The waveform of i_a is sinusoidal with less distortion, which indicates that the proposed repetitive control scheme can well suppress the undesired harmonic components.

Figures 11 and 12 show the steady-state harmonic compensation results with and without fractional delay compensation when the nonlinear load is connected, respectively. In Figure 11, the total harmonic distortion (THD) of the source current i_{sa} is reduced to 3.8% from 24.8% (THD of the load current), and the distortion ratio of 5th, 7th, 11th, and 13th harmonics in i_{sa} are reduced to 2.3%, 1.3%, 1.6%, and 1.2%, respectively. As a comparison, the THD of i_{sa} is 4.9% in Figure 12. These comparison experimental results demonstrate the good static performance of the $6k + 1$ repetitive controller and the effectiveness of the fractional delay compensation.

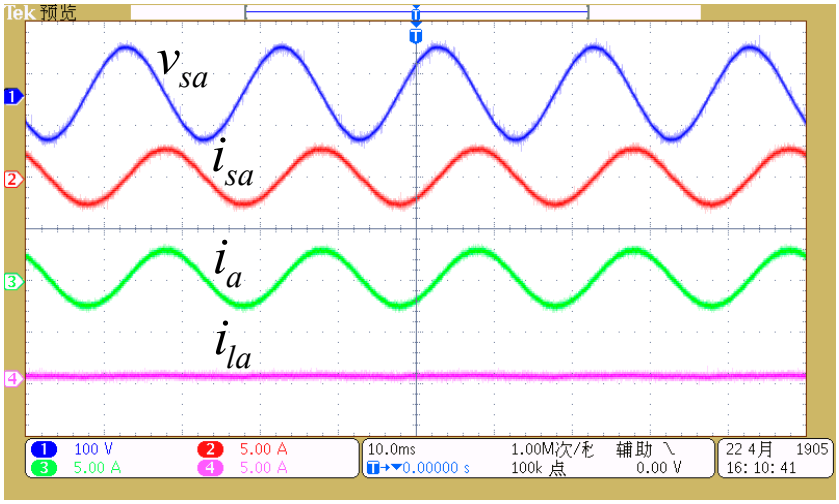

Figure 10. Harmonic compensation results with nonlinear load disconnected.

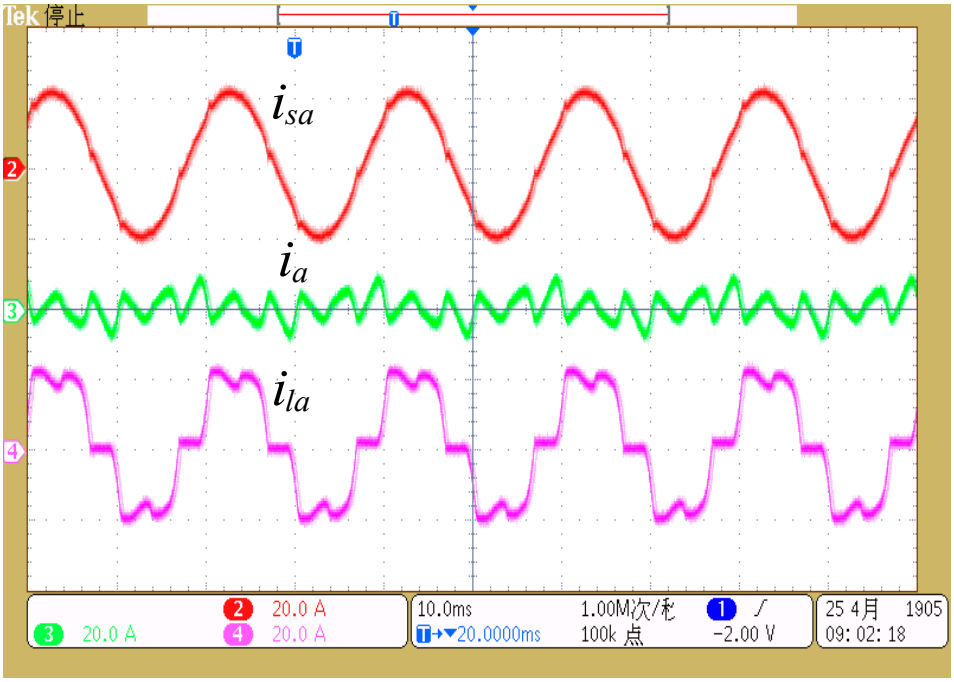

(**a**)

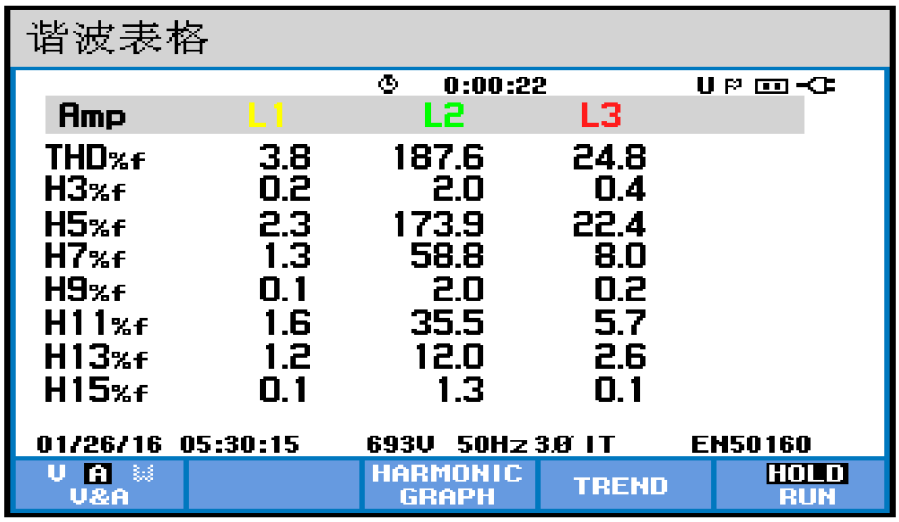

(**b**)

Figure 11. Harmonic compensation results with fractional delay (FD) compensation: (**a**) Source (L1), compensating (L2), load (L3) current waveforms; (**b**) Harmonic distortion rate graph.

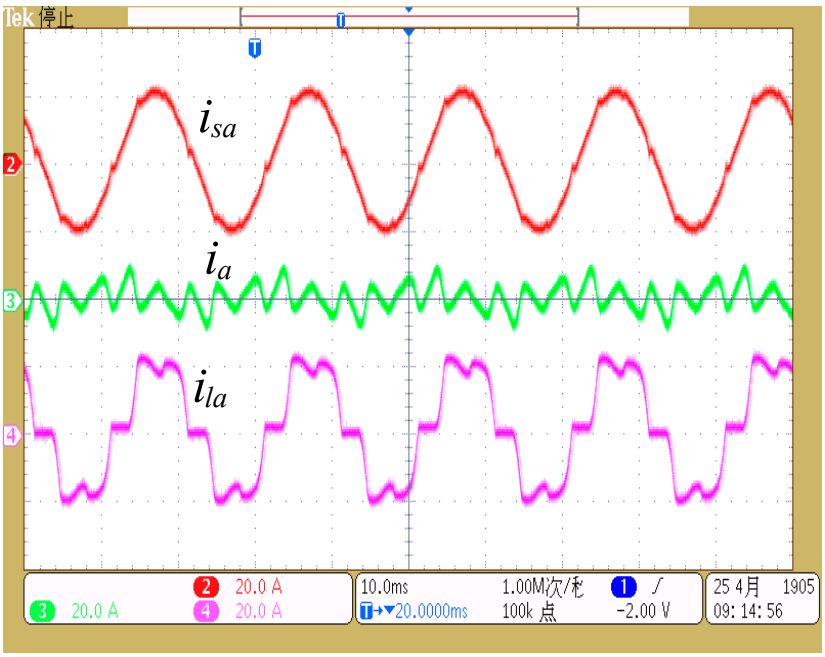

(**a**)

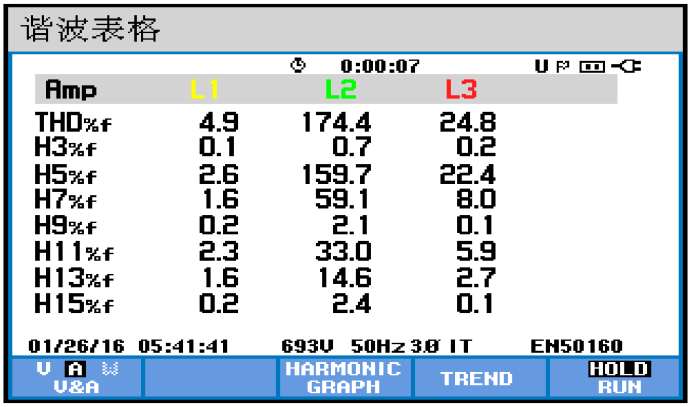

(**b**)

Figure 12. Harmonic compensation results without FD compensation: (**a**) Source (L1), compensating (L2), load (L3) current waveforms; (**b**) Harmonic distortion rate graph.

Also, to highlight the effectiveness of the $6k + 1$ repetitive control scheme, the harmonic compensation results by only the LC filter are shown in Figure 13. As seen, the source current is still highly distorted after the compensation of the LC filter, with a THD of 15.9%. The main reasons are that the resonant frequency of the LC filter is not precisely tuned at a domain harmonic frequency, and the performance of the LC filter seriously depends on the internal resistance of the grid source.

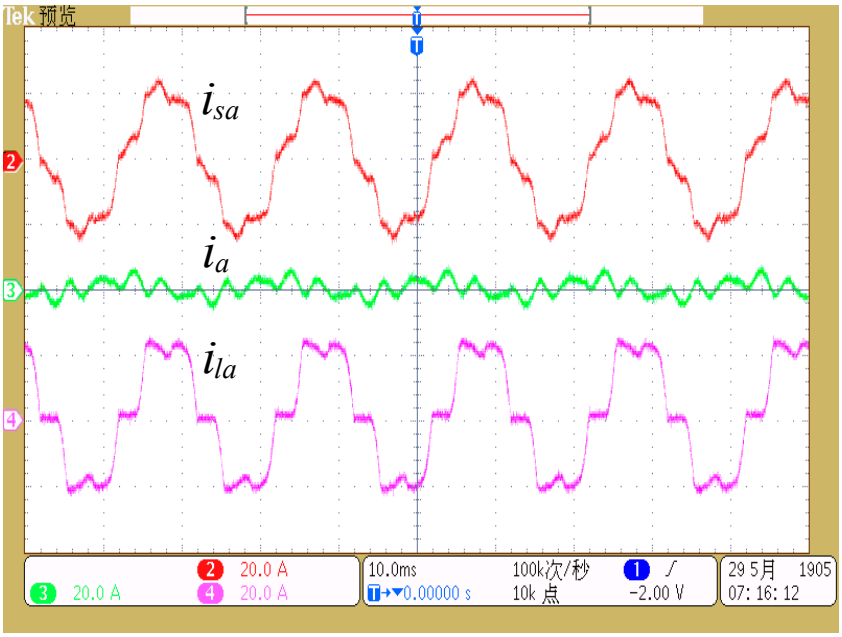

(**a**)

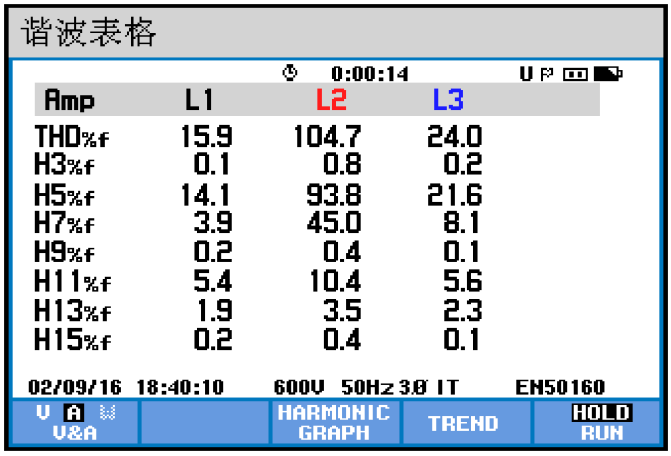

(**b**)

Figure 13. Harmonic compensation results by only the LC filter: (**a**) Source (L1), compensating (L2), load (L3) current waveforms; (**b**) Harmonic distortion rate graph.

To verify the dynamic performance of the $6k + 1$ repetitive control scheme, Figure 14 shows the comparison experimental results of the proposed and traditional repetitive control schemes in the transient process. As seen, before time t_1, the harmonic compensation function is not enabled, i_a is only the reactive power current provided by the LC filter with sinusoidal waveform, and i_{sa} is distorted by the load harmonics. At time t_1, the harmonic compensation function is enabled. The $6k + 1$ repetitive control scheme can take effect after $T_0/6$ time, and eliminate the steady-state error of harmonic tracking quickly. As a comparison, the traditional repetitive control scheme takes effect after T_0 time, and needs several T_0 periods to eliminate the steady-state error. The experimental results demonstrates that the $6k + 1$ repetitive control scheme has a much better dynamic performance than the traditional repetitive control scheme, which is consistent with the theoretical analysis.

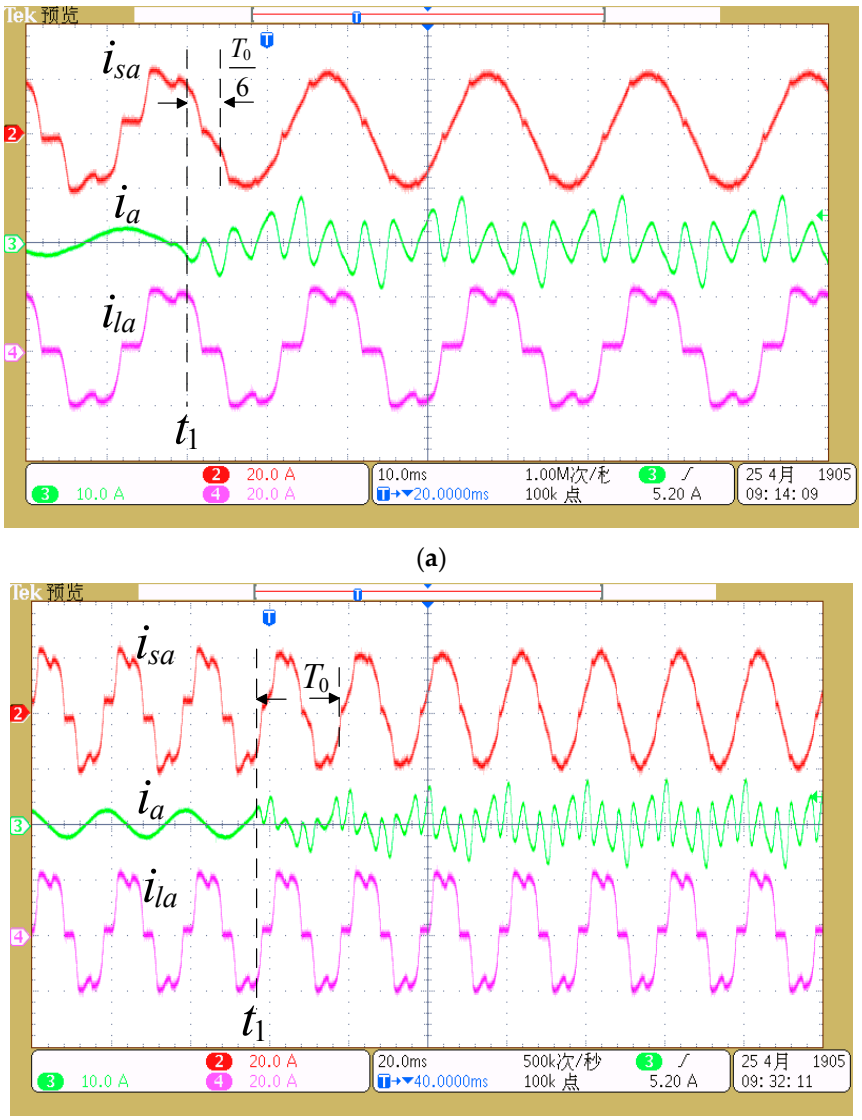

Figure 14. Dynamic performance comparison: (**a**) $6k + 1$ repetitive control scheme; (**b**) Traditional repetitive control scheme.

6. Conclusions

In this paper, a $6k + 1$ repetitive control scheme for HAPF is proposed, which aims at compensating the $6k + 1$ harmonics in three-phase power systems. The internal model of the $6k + 1$ repetitive controller is constructed on the general mathematical principles of a traditional repetitive controller, and expressed using the complex-vector notation. An FD compensating method for the $6k + 1$ repetitive controller is also presented. Through theoretical analysis and experiments, it was demonstrated that the $6k + 1$ repetitive control scheme can achieve a fast transient response with a delay time of $T_0/6$, and a good performance for compensating or suppressing the $6k + 1$ harmonics. Furthermore, due to the above features, the $6k + 1$ repetitive control scheme is also suitable to be used in current or voltage control for other three-phase grid-connected inverters.

Acknowledgments: This work was supported by the National Natural Science Foundation of China under Grant 51677195, the National High-tech R&D Program of China under Grant 2015AA050604, the Project of Innovation-driven Plan in Central South University.

Author Contributions: Zhaoxu Luo conceived the main idea and wrote the manuscript with guidance from Mei Su, Jian Yang and Yao Sun; Xiaochao Hou perforemed the experments. Josep M. Guerrero reviewed the work and given helpful improvement suggestions.

Conflicts of Interest: The authors declare no conflict of interest.

References

1. Singh, B.; Al-Haddad, K.; Chandra, A. A review of active filters for power quality improvement. *IEEE Trans. Ind. Electron.* **1999**, *46*, 960–971. [CrossRef]
2. Peng, F.Z. Application issues of active power filters. *IEEE Ind. Appl. Mag.* **1998**, *4*, 21–30. [CrossRef]
3. Trinh, Q.N.; Lee, H.H. An advanced current control strategy for three-phase shunt active power filters. *IEEE Trans. Ind. Electron.* **2013**, *60*, 5400–5410. [CrossRef]
4. Cao, W.; Liu, K.; Ji, Y.; Wang, Y.; Zhao, J. Design of a four-branch lcl-type grid-connecting interface for a three-phase, four-leg active power filter. *Energies* **2015**, *8*, 1606–1627. [CrossRef]
5. Bhattacharya, S.; Divan, D.M. Active filter solutions for utility interface of industrial loads. In Proceedings of the 1996 International Conference on Power Electronics, Drives and Energy Systems for Industrial Growth, New Delhi, India, 8–11 January 1996; pp. 1078–1084.
6. Bhattacharya, S.; Cheng, P.T.; Divan, D.M. Hybrid solutions for improving passive filter performance in high power applications. *IEEE Trans. Ind. Appl.* **1997**, *33*, 732–747. [CrossRef]
7. Inzunza, R.; Akagi, H. A 6.6-kV transformerless shunt hybrid active filter for installation on a power distribution system. *IEEE Trans. Power Electron.* **2005**, *20*, 893–900. [CrossRef]
8. Lee, T.L.; Wang, Y.C.; Li, J.C. Hybrid active filter with variable conductance for harmonic resonance suppression in industrial power systems. *IEEE Trans. Ind. Electron.* **2015**, *62*, 746–756. [CrossRef]
9. Luo, Z.X.; Su, M.; Sun, Y.; Zhang, W.; Lin, Z.L. Analysis and control of a reduced switch hybrid active power filter. *IET Power Electron.* **2016**, *9*, 1416–1425. [CrossRef]
10. Luo, A.; Xu, X.Y.; Fang, H.H. Feedback-feedforward PI-type iterative learning control strategy for hybrid active power filter with injection circuit. *IEEE Trans. Ind. Electron.* **2010**, *57*, 3767–3779. [CrossRef]
11. Deng, Y.P.; Tong, X.Q.; Jia, H. A bidirectional control principle of active tuned hybrid power filter based on the active reactor using active techniques. *IEEE Trans. Ind. Inform.* **2015**, *11*, 141–154. [CrossRef]
12. Zou, Z.X.; Zhou, K.L.; Wang, Z. Frequency-adaptive fractional-order repetitive control of shunt active power filters. *IEEE Trans. Ind. Electron.* **2015**, *62*, 1659–1668. [CrossRef]
13. Sun, J.J.; Gong, J.W.; Chen, B.F. Analysis and design of repetitive controller based on regeneration spectrum and sensitivity function in active power filter system. *IET Power Electron.* **2014**, *7*, 2133–2140. [CrossRef]
14. Miret, J.; Castilla, M.; Matas, J. Selective harmonic-compensation control for single-phase active power filter with high harmonic rejection. *IEEE Trans. Ind. Electron.* **2009**, *56*, 3117–3127. [CrossRef]
15. Grino, R.; Cardoner, R.; Castelló, C.R. Digital repetitive control of a three-phase four-wire shunt active filter. *IEEE Trans. Ind. Electron.* **2007**, *54*, 1495–1503. [CrossRef]
16. Castelló, C.R.; Grino, R.; Fossas, E. Odd-harmonic digital repetitive control of a single-phase current active filter. *IEEE Trans. Power Electron.* **2004**, *19*, 1060–1068. [CrossRef]
17. Escobar, G.; Martinez, P.R.; Ramos, L.J. A Negative feedback repetitive control scheme for harmonic compensation. *IEEE Trans. Ind. Electron.* **2006**, *53*, 1383–1386. [CrossRef]
18. Escobar, G.; Hernandez-Briones, P.G.; Martinez, P.R. A repetitive-based controller for the compensation of 6l $\pm$ 1 harmonic components. *IEEE Trans. Ind. Electron.* **2008**, *55*, 3150–3158. [CrossRef]
19. Chen, D.; Zhang, J.M.; Qian, Z.M. Research on fast transient and 6n $\pm$ 1 harmonics suppressing repetitive control scheme for three-phase grid-connected inverters. *IET Power Electron.* **2013**, *6*, 601–610. [CrossRef]
20. Escobar, G.; Gomez, H.M.; Valdez-Fernandez, A.A. Implementation of a 6n $\pm$ 1 repetitive controller subject to fractional delays. *IEEE Trans. Ind. Electron.* **2015**, *62*, 444–452. [CrossRef]